JACS
JOURNAL OF THE AMERICAN CHEMICAL SOCIETY

Article

pubs.acs.org/JACS

Self-Assembly of Metal Phenolic Mesocrystals and Morphosynthetic Transformation toward Hierarchically Porous Carbons

Seung Jae Yang, Markus Antonietti, and Nina Fechler*

Department of Colloid Chemistry, Max Planck Institute of Colloids and Interfaces, MPI Campus Golm, Am Mühlenberg 1, 14476 Potsdam, Germany

Supporting Information

ABSTRACT: A facile and sustainable synthetic strategy based on the coordination of natural polyphenols with metal ions is developed for the textural engineering of mesocrystals and hierarchical carbon nanomaterials. The desired control of coordination between ellagic acid and zinc ions enables the macroscopic self-assembly behavior of crystalline nanoplatelets to be tailored into round and elongated "peanut"-like micron-sized mesostructured particles. Direct carbonization of these mesocrystals generates hierarchically porous carbon particles in good yields, possessing bimodal micro- and mesoporous architecture along with a well-preserved macroscopic structure. The pore system provides both small storage sites, demonstrated by high CO_2 uptake, and transport channels also accessible by larger molecules.

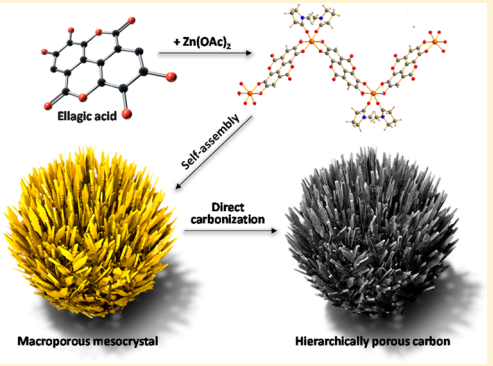

INTRODUCTION

Due to their ubiquitous properties, nanostructured porous carbon materials are of particular interest in addressing global energy and environmental issues.[1] Typical synthesis methods involving soft and hard templating can produce micro- or mesoporous carbon materials with well-defined pores.[1,2] However, in the past decade, the desire for a multivariable performance of porous carbon materials stimulated much effort to explore hierarchical pore architectures.[3] Besides others, these provide rapid pore-transport systems and make these materials suitable for real-life applications where fast response at high performance is essential. To realize such structures, several approaches have been suggested, including the incorporation of mesopore-generating templates into microporous carbon, chemical activation of mesoporous carbon for introducing microporosity, or even complete nanoreplication using colloidal silica and polymer beads.[2,4] Even though these methods have enabled the successful preparation of hierarchically porous carbons, the described routes are admittedly rather academic and not competitive due to the complicated processing and price. Recent advances in carbon science, which combine three-dimensionally assembled structure formation or inclusion of multiple templates, allowed for the synthesis of hierarchically porous carbons with a macroscopic pore network.[2a,3d,4] However, these approaches required laborious and complicated steps, involving physicochemical activation for micro- and mesopores or additional steps to remove the template without collapse of the original pore structure. Taken together, the development of template-free and facile methods to synthesize hierarchically porous carbon structures, eventually even endowing enhanced functionality, is highly desirable.

Bioinspired materials based on coordination between metals and biomolecules have shown miscellaneous self-assembly behaviors with exceptional features.[5] Stimulated by this bioinspired process, we herein demonstrate a template-free alternative synthesis approach for porous carbons with unique pore structure and morphology derived from hierarchically assembled materials based on zinc−polyphenol coordination, here exemplified with the model compound ellagic acid (EA).

RESULTS AND DISCUSSION

In the first step, we synthesized three-dimensional crystalline microparticles from zinc (Zn) ions coordinated to EA, a well-known edible natural product, for instance, contained as a major component in cranberries. This polyphenol−Zn ion complex not only possesses strong and directed coordination to allow for the formation of a very well organized framework, which assembles into mesocrystals, but can be further transformed into the respective carbon under full structure retention after high-temperature treatment. Here, it is noted that structural replication of precursor structures into carbons, on the one hand, relies on low volatility and high carbonization yields, and the partially ionic characteristic of such complexes, contrary to the primary phenols, ensures a very efficient carbonization. On the other hand, thermal conversion of such structures generates not only carbons but also inherently corresponding metal oxide clusters that can act as "localized" inner templates and leaving groups, ensuring the effective use of the zinc−EA crystal as a carbon precursor and porogen, that is, "all-in-one" unit. In other words, carbonizing metal phenolic

Received: April 30, 2015
Published: June 10, 2015

DOI: 10.1021/jacs.5b04500
J. Am. Chem. Soc. 2015, 137, 8269−8273

polymers and frameworks combines the recently described techniques of carbonizing ionic liquids with the "salt-templating" approach.[1e] As illustrated in Scheme 1, in *N*-methyl-2-pyrrolidone (NMP) as solvent and at ambient temperature and pressure, the EA building units are linked by Zn ions to form a robust framework, giving control over several length scales.

Scheme 1. Synthetic Procedures for the Zinc–Elagic Acid Mesocrystals and Their Hierarchically Porous Carbon

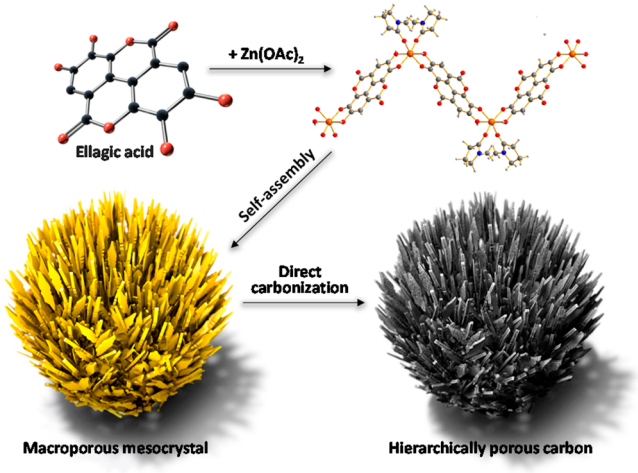

The compound from EA and zinc acetate dehydrate and its mesocrystals were spontaneously formed by mixing their NMP solutions in a 1:2 molar ratio at room temperature. The crystals/carbons are denoted as EAZn2_Xd_C, where 2 refers to the molar ratio of EA/Zn, X is the crystallization time in days, and C indicates carbonization. The successful coordination between EA and the Zn ion is indicated by the vanishing of characteristic O–H vibration peaks of the EA in the Fourier transform infrared (FT-IR) spectra of the EAZn2 mesocrystal (Supporting Information Figure S1).[6] The morphology was characterized by optical microscopy (OM) and scanning electron microscopy (SEM), and representative pictures are shown in Figure 1. OM images (Figure 1a) reveal that the products consist of microparticles of uniform size and distribution with an average particle diameter of approximately 6 μm. Polarized optical microscopy images (inset of OM image Figure 1a) indicate strong birefringence, and clear Maltese crosses are observed, indicative of a radial symmetry as, for instance, found in polymer spherulite-like crystals.[7] This crystallinity is further confirmed by sharp X-ray diffraction (XRD) patterns of the microparticles, which are distinct from the two precursors (Supporting Information Figure S2). A survey SEM micrograph (Figure 1b) shows aggregated microparticles of uniform size, consistent with OM results. To further determine the detailed microstructure evolution of these microparticles, the higher-magnification SEM micrographs are presented in Figure 1c,d. Very interestingly, the surfaces of the microparticles consist of loosely packed nanoplatelets that are aligned parallel to the sphere pointing to the same center. Eventually, spherical structures with an equatorial rim are formed, figuratively comparable with a distorted "pokeball" (Figure 1d and Supporting Information Figure S3 for further SEM and transmission electron microscopy, TEM).[8]

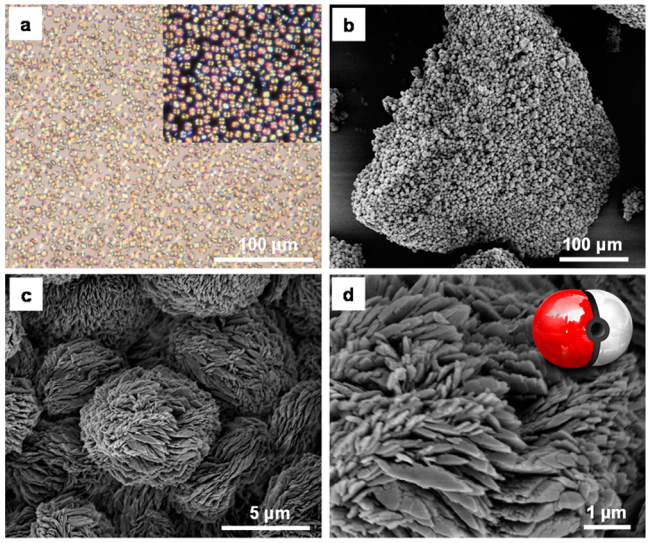

Figure 1. (a) OM image (inset: polarized OM image) and (b–d) SEM micrographs of EAZn2_2d mesocrystals.

To gain insights into the formation mechanism of these mesocrystalline microparticles, we monitored their time-dependent formation behavior by OM with polarized light, SEM, and XRD. The transparent colorless solution mixture changed quickly to yellow, followed by the formation of small mesocrystalline particles embedded in an amorphous gel matrix (Supporting Information Figures S4 and S5). As the reaction time increases, the amorphous gel matrix disappears and new mesocrystals are generated simultaneously. The mesocrystals continuously grew to approximately 6 μm in diameter after 2 days; afterward, they continued to grow slower and in the longitudinal direction, forming peanut-like particles (Figure 2a,b and Supporting Information Figures S4 and S6a,b).[9] This behavior was also observed for other mesocrystalline materials;[9] however, here we indeed have an organic-based entity. This nicely shows the dynamic, adaptive characteristics of this system, probably provided by the supramolecular characteristics of the primary links.

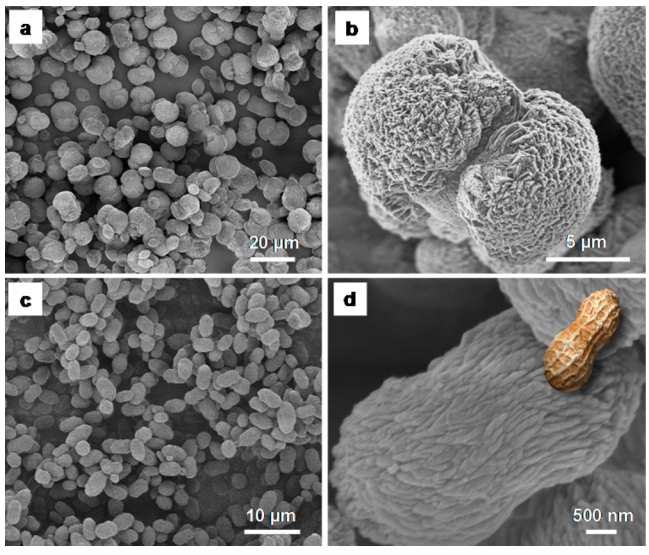

Figure 2. SEM micrographs of (a,b) EAZn2_7d and (c,d) EAZn1_2d mesocrystals.

DOI: 10.1021/jacs.5b04500
J. Am. Chem. Soc. 2015, 137, 8269–8273

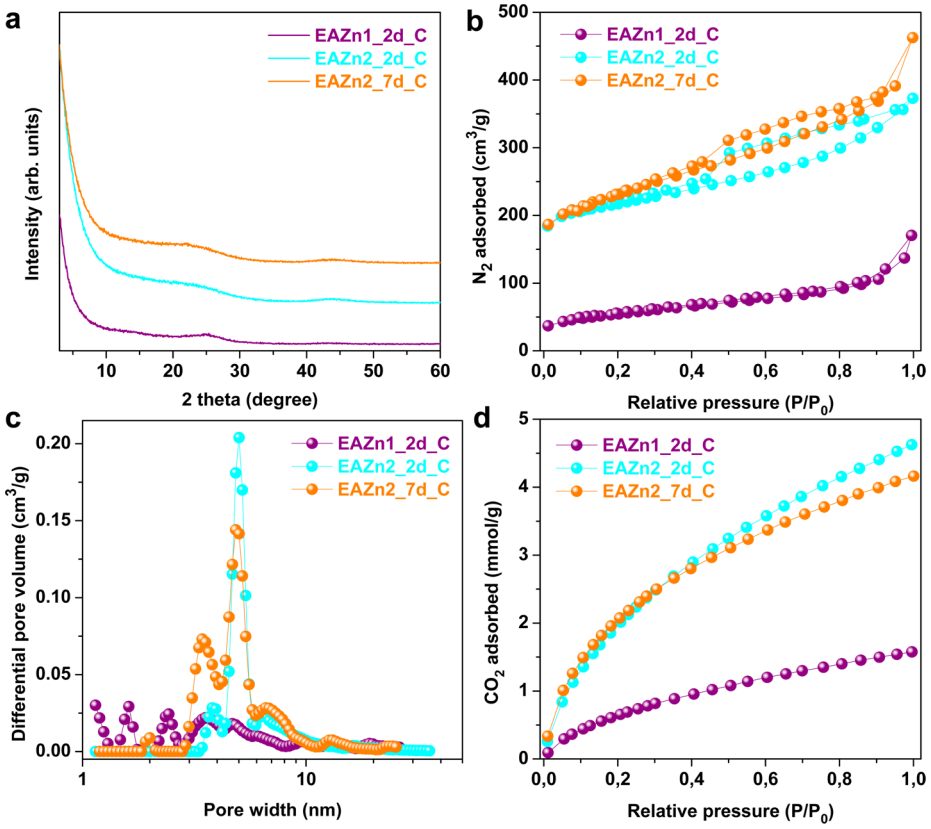

Figure 3. (a) XRD patterns, (b) nitrogen isotherms at 77 K, (c) pore size distribution calculated from nitrogen isotherms with the quenched solid density functional theory model, and (d) CO_2 adsorption at 273 K of the obtained mesocarbon materials.

We then investigated the effect of the Zn ion concentration on the morphological evolution of the mesocrystal. Concentration of metal ions usually has a large influence in biomineralization and construction in complex materials.[8,10] Indeed, using equimolar NMP solutions of EA and the zinc acetate leads to the spontaneous formation of highly uniform elongated, peanut-like crystals (Figure 2c,d and Supporting Information Figure S7). In contrast to the EAZn2 crystal, the whole surface of the EAZn1 crystal is composed of densely packed nanoplatelets with regular ordering, leading to a much smoother and denser mesocrystal structure. It is noted that the concentration of the Zn ion modulates the self-assembly behavior of the mesocrystal, however, without any change of physical and chemical structures (Figure S8); that is, the crystals still show the same stoichiometry. Due to the simplicity of this metal polyphenol coordination approach, it may offer a new system to synthesize programmable hierarchically ordered materials. We also speculate that the known high functionality of polyphenols is transferable to the properties of the assemblies.

The synthesis of the hierarchically porous carbon microparticles (denoted as mesocarbon) was achieved by a facile direct carbonization (≥900 °C) of the bioinspired mesocrystals without any further external templating or washing steps. The successful transformation of the mesocrystals to a carbon species was confirmed by XRD studies (Figure 3a). Here, the low signal intensities point to a weakly stacked pattern; that is, the molecular crystal structure is essentially kept in the carbon, avoiding macroscopic restacking. During the heating process to 800 °C, the coordination bonds between Zn ions and EA in the mesocrystals turned into the carbonaceous framework and equimolar amounts of ZnO (Supporting Information Figure S9), thus keeping the ionic charge balanced. The as-formed ZnO clusters tightly mix with the carbon and act as a local template. Further temperature increase can lead to the reduction of ZnO nanoparticles in the presence of carbon materials (carbothermal reduction), accompanied by the evaporation of Zn, CO_2, and CO. This "controlled molecular etching" not only removes all inorganic compounds without the necessity of washing but also results in accessible nanoscale porosity.[11] The fact that the as-formed reduced Zn metal is easily vaporized throughout heating at 900 °C for 1 h was confirmed by finding a negligible amount of remaining Zn metal in the carbon matrix with inductively coupled plasma optical emission spectrometry (Zn < 0.3 wt %). Further investigation on the composition by combustion elemental analysis indicates that the obtained material is mainly composed of carbon atoms (93.41 wt % C, 1.23 wt % N, and 1.17 wt % H), which supports very nicely the proposed elimination scheme.

Cryogenic N_2 sorption revealed combined characteristics of types I and IV isotherms, in which a steep increase was observed at low relative pressures, followed by a moderate increase at intermediate relative pressures accompanied by a desorption hysteresis (Figure 3b). This highlights the formation of a hierarchical pore architecture consisting of micro- and mesopores (Table 1).[11,12] Less developed or accessible porosity of the EAZn1_C mesocarbon might be attributed to the more densely packed assembled mesocrystal morphology (Figure 2d and Supporting Information Figure S7). The calculation of the pore size distribution, which was performed using quenched solid density functional theory, indicated the formation of

DOI: 10.1021/jacs.5b04500
J. Am. Chem. Soc. 2015, 137, 8269−8273

Table 1. Textural Characteristics of the Mesocrystals and Respective Mesocarbons

material	S_{BET} [a] ($m^2\ g^{-1}$)	S_{micro} [b] ($m^2\ g^{-1}$)	S_{meso} [c] ($m^2\ g^{-1}$)	pore volume ($cm^3\ g^{-1}$)
EAZn1_2d	27			0.09
EAZn2_2d	31			0.06
EAZn1_2d_C	202	40	155	0.26
EAZn2_2d_C	829	503	326	0.58
EAZn2_7d_C	842	435	407	0.72

[a]Determined by BET equation. [b]Micropore surface area calculated from *t* plots. [c]Mesopore surface area.

nearly uniform mesopores of approximately 5 nm in diameter for EAZn2_2d_C (Figure 3c and Supporting Information Figure S10). In the case of EAZn2_7d_C, a bimodal pore size distribution is found, with additional pores centered around 4 nm, which can originate from the different crystal habitus in the fusion zone (Figure 2 and Supporting Information Figure S6). In contrast, for EAZn1_2d_C, mainly micropores and a lower surface area are found, which is in accordance with the denser overall microstructure revealed by the other measurement techniques shown above. Further investigation of CO_2 uptake at 273 K (Figure 3d) shows that the developed microporosity is mainly due to ultramicropores (pore width <1 nm), strongly governing the amount of CO_2 uptake.[13] Note that the found values of 4.6 and 4.2 mmol g^{-1} for EAZn2_2d_C and EAZn2_7d_C, respectively, outperform widely used benchmark microporous materials such as metal–organic frameworks and activated carbons with their much higher specific surface areas (SSA) exceeding 2000 $m^2\ g^{-1}$.[14] Because the experimental SSAs of the mesocarbons are found to be below 1000 $m^2\ g^{-1}$, these adsorption values emphasize the importance and suitability of the textural pore characteristics that likely result from hindered carbon restacking provided by the mesocrystal and functionality for CO_2 adsorption (Supporting Information Figure S11). Additionally, very small micropores, which are not accessible by nitrogen, can be reached by CO_2, which would fit the picture of a molecular zinc oxide salt template fraction.

SEM micrographs indicate that the morphology of the synthesized mesocrystals can be retained even after high-temperature carbonization, leading to the transcription of the metal–polyphenol assembly into its carbon equivalent (Figure 4a,b and Supporting Information Figure S12). When we take into account the macroporosity also present in the primary crystals and their replicas, which is, however, not detectable by conventional N_2 sorption but only visible from SEM micrographs, these carbons indeed possess a hierarchical porosity over several length scales. This suggests that a three-dimensional bicontinuous macroscale pore network from the porous carbon nanoplatelet assembly can be accomplished, which is, in general, highly advantageous for mass transport. Even the less porous EAZn1_2d_C mesocarbon displayed macroscale porosity, in spite of its more ordered nanoplatelet assembly (Supporting Information Figure S12). Further confirmation of the well-developed pore structure was given by TEM, presenting internal voids and nonspherical hollow structures (Figure 4c).

To further illustrate the structural merits of this unique pore architecture, we also explored the adsorption behavior of larger molecules. As an example, Rhodamine B (RhB) dye removal was examined, particularly in comparison with a typical microporous nitrogen-doped carbon (denoted as Micro C)

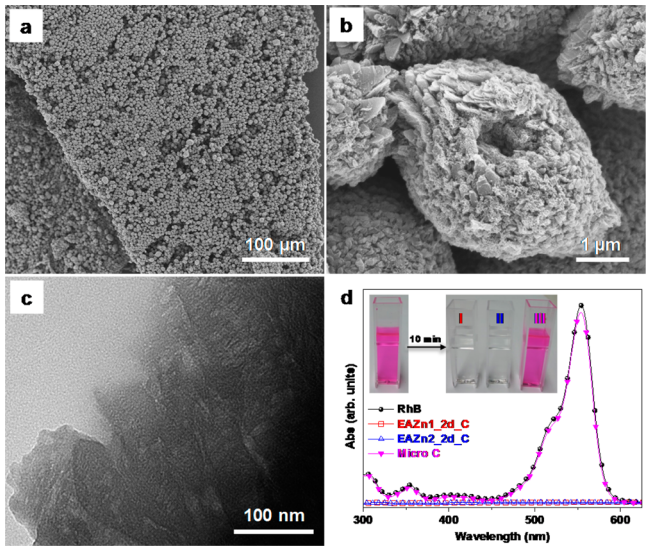

Figure 4. (a,b) SEM micrographs and (c) TEM micrograph of EAZn2_2d_C mesocarbon. (d) UV–vis absorption of Rhodamine B (RhB) solutions with various products after 10 min mixing under dark conditions. Inset of (d): Photograph of RhB solutions, where I, II, and III correspond to the addition of equal mass amounts of the carbons EAZn1_2d_C, EAZn2_2d_C, and Micro C mixtures, respectively.

fabricated by the salt-templating method, possessing a high surface area (>1500 $m^2\ g^{-1}$; see Supporting Information Figure S13) and a nitrogen content of 11.77 wt % but no mesopores. As shown in Figure 4d, very fast RhB adsorption (maximum adsorption capacities for EAZn1_2d_C and EAZn2_2d_C are 70 and 110 mg g^{-1}, respectively, in 10 min; adsorption of the products is almost saturated) is observed for the porous mesocarbons derived from the Zn–oligophenol complexes (Figure 4d, I and II), whereas the RhB solution containing the microporous reference material remained unaffected even after 1 h (Figure 4d, III, and Supporting Information Figure S14). Taking into account that the reference material possesses a 10 times higher nitrogen content and twice the apparent surface area compared to the mesocrystal-derived carbons (11.77 wt % N for Micro C vs 1.23 wt % N for EAZn2_2d_C), this result proves that the presence of sufficiently large mesopores is essential. A small amount of RhB adsorption was also found in the macroporous mesocrystals (maximum adsorption capacities for EAZn1_2d and EAZn2_2d are 6 and 5 mg g^{-1}, respectively, in 10 min), which further supports an importance of a hierarchic pore system for storing a high amount of large-scale molecules. The higher uptake of the respective carbons is attributed to the additional pores which are freed during the thermal treatment. Eventually, the hierarchical morphology also enables shortened transport for a relatively large molecule from the external surface to the interior surface, minimizing adsorption time. Considering the versatility of available natural oligo- and polyphenols and their combination with different metal ions, this synthesis with the benign and facile conditions offers a more sustainable, facile approach toward unique carbon structures.

CONCLUSION

In conclusion, we have demonstrated the synthesis of mesocrystalline microparticles constituted by the self-assembly of zinc ions and the natural polyphenol ellagic acid. The control of relative stoichiometry enabled the macroscopic tailoring

DOI: 10.1021/jacs.5b04500
J. Am. Chem. Soc. 2015, 137, 8269–8273

from round and elongated "peanut"-like micron-sized mesostructured particles while keeping the crystal structure constant. These unique structures could be transformed into the corresponding hierarchically porous carbon microparticles with high carbonization yields under retention of the macroscopic mesostructure simply by being thermally annealed without any additional templating or washing steps. This was explained by the well-chosen composition and reactivity of the (nonvolatile) primary Zn−oligophenol complexes, which constitutes a carbon precursor and an ionic salt template "all-in-one" structure. The resulting carbon materials exhibited a pore architecture with controlled pore sizes over several length scales from micro- to meso- to macropores. This equips these materials with promising properties such as high mass transport and uptake, which were representatively shown not only for the high CO_2 gas adsorption (quantifying microporosity) but also by the quick removal of larger molecules such as RhB (quantifying mesoporosity and pore-transport system). Taking into account the multifarious availability of natural polyphenols and their combination with the desired metal ions, we believe that the presented approach will open a broad alternative and sustainable platform toward unique self-assembly morphologies and the consecutive design of carbon nanomaterials possessing distinct structural and functional features.

■ ASSOCIATED CONTENT

Supporting Information

Additional experimental details, synthesis, and characterizations. The Supporting Information is available free of charge on the ACS Publications website at DOI: 10.1021/jacs.5b04500.

■ AUTHOR INFORMATION

Corresponding Author

*nina.fechler@mpikg.mpg.de

Notes

The authors declare no competing financial interest.

■ ACKNOWLEDGMENTS

The authors would like to thank Prof. Uwe Schilde from the University of Potsdam for assistance with single-crystal measurements, Rona Pitschke for ultramicrotome TEM measurements, Dr. Andreas Holländer for XPS measurements, and Yoobin Chun for support with figure design.

■ REFERENCES

(1) (a) Hu, B.; Wang, K.; Wu, L.; Yu, S.-H.; Antonietti, M.; Titirici, M.-M. *Adv. Mater.* **2010**, *22*, 813. (b) Yang, W.; Fellinger, T.-P.; Antonietti, M. *J. Am. Chem. Soc.* **2011**, *133*, 206. (c) Liang, C.; Li, Z.; Dai, S. *Angew. Chem., Int. Ed.* **2008**, *47*, 3696. (d) Meng, Y.; Gu, D.; Zhang, F.; Shi, Y.; Yang, H.; Li, Z.; Yu, C.; Tu, B.; Zhao, D. *Angew. Chem., Int. Ed.* **2005**, *44*, 7053. (e) Zhang, S.; Dokko, K.; Watanabe, M. *Mater. Horiz.* **2015**, *2*, 168. (f) Lee, J.; Kim, J.; Hyeon, T. *Adv. Mater.* **2006**, *18*, 2073.

(2) (a) Lee, H. I.; Stucky, G. D.; Kim, J. H.; Park, C.; Chang, H.; Kim, J. M. *Adv. Mater.* **2011**, *23*, 2357. (b) Fang, Y.; Lv, Y.; Gong, F.; Wu, Z.; Li, X.; Zhu, H.; Zhou, L.; Yao, C.; Zhang, F.; Zheng, G.; Zhao, D. *J. Am. Chem. Soc.* **2015**, *137*, 2808. (c) Talapaneni, S. N.; Mane, G. P.; Mano, A.; Anand, C.; Dhawale, D. S.; Mori, T.; Vinu, A. *ChemSusChem* **2012**, *5*, 700. (d) Lee, J.; Yoon, S.; Hyeon, T.; Oh, S. M.; Kim, K. B. *Chem. Commun.* **1999**, *21*, 2177.

(3) (a) Hu, Y.-S.; Adelhelm, P.; Smarsly, B. M.; Hore, S.; Antonietti, M.; Maier, J. *Adv. Funct. Mater.* **2007**, *17*, 1873. (b) Yang, S. J.; Kim, T.; Lee, K.; Kim, Y. S.; Yoon, J.; Park, C. R. *Carbon* **2014**, *71*, 294. (c) Zhang, J.; Qiao, Z.-A.; Mahurin, S. M.; Jiang, X.; Chai, S.-H.; Lu, H.; Nelson, K.; Dai, S. *Angew. Chem., Int. Ed.* **2015**, *54*, 4582. (d) Oschatz, M.; Borchardt, L.; Thommes, M.; Cychosz, K. A.; Senkovska, I.; Klein, N.; Frind, R.; Leistner, M.; Presser, V.; Gogotsi, Y.; Kaskel, S. *Angew. Chem., Int. Ed.* **2012**, *51*, 7577.

(4) (a) Fulvio, P. F.; Mayes, R. T.; Wang, X.; Mahurin, S. M.; Bauer, J. C.; Presser, V.; McDonough, J.; Gogotsi, Y.; Dai, S. *Adv. Funct. Mater.* **2011**, *21*, 2208. (b) Deng, Y.; Cai, Y.; Sun, Z.; Gu, D.; Wei, J.; Li, W.; Guo, X.; Yang, J.; Zhao, D. *Adv. Funct. Mater.* **2010**, *20*, 3658. (c) Itoi, H.; Nishihara, H.; Kogure, T.; Kyotani, T. *J. Am. Chem. Soc.* **2011**, *133*, 1165. (d) Deng, Y.; Yu, T.; Wan, Y.; Shi, Y.; Meng, Y.; Gu, D.; Zhang, L.; Huang, Y.; Liu, C.; Wu, X.; Zhao, D. *J. Am. Chem. Soc.* **2007**, *129*, 1690.

(5) (a) Guo, J.; Ping, Y.; Ejima, H.; Alt, K.; Meissner, M.; Richardson, J. J.; Yan, Y.; Peter, K.; Von Elverfeldt, D.; Hagemeyer, C. E.; Caruso, F. *Angew. Chem., Int. Ed.* **2014**, *53*, 5546. (b) Harrington, M. J.; Masic, A.; Holten-Andersen, N.; Waite, J. H.; Fratzl, P. *Science* **2010**, *328*, 216. (c) Yu, S.-H.; Cölfen, H.; Tauer, K.; Antonietti, M. *Nat. Mater.* **2005**, *4*, 51. (d) Ejima, H.; Richardson, J. J.; Liang, K.; Best, J. P.; Van Koeverden, M. P.; Such, G. K.; Cui, J.; Caruso, F. *Science* **2013**, *341*, 154.

(6) Zhang, P.; Li, H.; Veith, G. M.; Dai, S. *Adv. Mater.* **2015**, *27*, 234.

(7) Watanabe, K.; Iida, H.; Akagi, K. *Adv. Mater.* **2012**, *24*, 6451.

(8) Liu, Z.; Wen, X. D.; Wu, X. L.; Gao, Y. J.; Chen, H. T.; Zhu, J.; Chu, P. K. *J. Am. Chem. Soc.* **2009**, *131*, 9405.

(9) (a) Wang, T.; Mitchell, J.; Börner, H.; Cölfen, H.; Antonietti, M. *Phys. Chem. Phys. Chem.* **2010**, *12*, 11984. (b) Xuan, S.; Hao, L.; Jiang, W.; Song, L.; Hu, Y.; Chen, Z.; Fei, L.; Li, T. *Cryst. Growth Des.* **2007**, *7*, 430.

(10) Xu, A. W.; Ma, Y.; Cölfen, H. *J. Mater. Chem.* **2007**, *17*, 415.

(11) (a) Liu, B.; Shioyama, H.; Akita, T.; Xu, Q. *J. Am. Chem. Soc.* **2008**, *130*, 5390. (b) Yang, S. J.; Kim, T.; Im, J. H.; Kim, Y. S.; Lee, K.; Jung, H.; Park, C. R. *Chem. Mater.* **2012**, *24*, 464.

(12) (a) Fechler, N.; Fellinger, T.-P.; Antonietti, M. *Adv. Mater.* **2013**, *25*, 75. (b) Kuhn, P.; Forget, A.; Su, D.; Thomas, A.; Antonietti, M. *J. Am. Chem. Soc.* **2008**, *130*, 13333.

(13) Presser, V.; McDonough, J.; Yeon, S.-H.; Gogotsi, Y. *Energy Environ. Sci.* **2011**, *4*, 3059.

(14) (a) Hong, D. H.; Suh, M. P. *Chem.—Eur. J.* **2014**, *20*, 426. (b) Fracaroli, A. M.; Furukawa, H.; Suzuki, M.; Dodd, M.; Okajima, S.; Gándara, F.; Reimer, J. A.; Yaghi, O. M. *J. Am. Chem. Soc.* **2014**, *136*, 8863. (c) Choi, S.; Drese, J. H.; Jones, C. W. *ChemSusChem* **2009**, *2*, 796.

DOI: 10.1021/jacs.5b04500
J. Am. Chem. Soc. 2015, 137, 8269−8273